

# Numerical Investigation of Fluid Flow Inside A Rectangular Driven Cavity at Moderate Reynolds Numbers

Pantha Pradip Das<sup>1,\*</sup>, Kalyan Kumar Das<sup>2</sup>

<sup>1,2</sup>Department of Mechanical Engineering, Assam Engineering College, Guwahati, Assam, India

## Abstract

This work presents a numerical investigation of a 2-D incompressible driven cavity flow at moderate Reynolds numbers. Lid driven cavity is widely considered to be a benchmark problem because of its capability of displaying the cogency of different numerical schemes and easily analysing different fluid phenomenon in a simple geometrical arrangement. A steady numerical solution is determined using a pressure-based segregated algorithm; SIMPLE and the simulation is done in the commercially available CFD software ANSYS FLUENT (Academic Version 18.1). The flow is studied for various aspect ratios ( $1 \leq K \leq 4$ ) at moderate Reynolds numbers 100, 400, 1000, 3200 and 5000 in uniform cartesian grids. The events mainly characterizing developments in primary and secondary vortices, their locations and the velocity profile are explained in detail. Moreover, an effort has been made to show the merging of corner vortices to a new primary vortex for different Reynolds number and also compute the critical aspect ratio ( $K_{cr}$ ) value for Reynolds number 50, 100 and 400. The results obtained in this work are compared with standards given by Ghia *et al.* and a good agreement of the result is observed.

**Keywords:** Lid driven cavity, 2-D incompressible, SIMPLE, Reynolds number, aspect ratio, critical aspect ratio

\*Author for Correspondence E-mail: panthadas4@gmail.com

## INTRODUCTION

This research is introduced in order to analyse one of the most important and widely used problem in CFD; the lid driven cavity problem. As hundreds of researches have authenticated, the driven cavity problem has been used as a definitive way to examine newly developed computational schemes. Here described the flow inside a rectangular cavity whose top surface is moving with a constant velocity and other surfaces are stationary. The behaviour of flow inside cavity for various Reynolds number and at different aspect ratios are investigated using the SIMPLE algorithm.

The concept of a driven cavity flow can directly be related to many industrial applications. For example, in the processing techniques for creating very fine-scale polymer composites and chaotic mixing in cylindrical cavity (as observed by Zumbrennen *et al.* [1]), where the 3-D flow field is a direct relevance of the driven cavity

flow. Also the cavity flow can be related to different working processes of industrial devices like short-dwell coaters and flexible blade coaters which are used for the production of high grade paper and photographic film [2]. In a short-dwell coater the undesirable affect on the coating quality and the coat weight profile due to the irrotational eddies inside the upstream pond of the blade was indicated by Aidun *et al.* [2] (Figure 1). The concept of cavity flow also serves as a basic phenomenon in melt-spinning processes performed while manufacturing metal ribbons of micro-crystalline materials [2]. This flow system is also seen in applications like flow over cut-outs and in the study of heat transfer due to repeated slots on the walls of heat exchangers [3].

Since 1966, this problem has been studied by researchers using different discretization schemes for different Reynolds numbers.

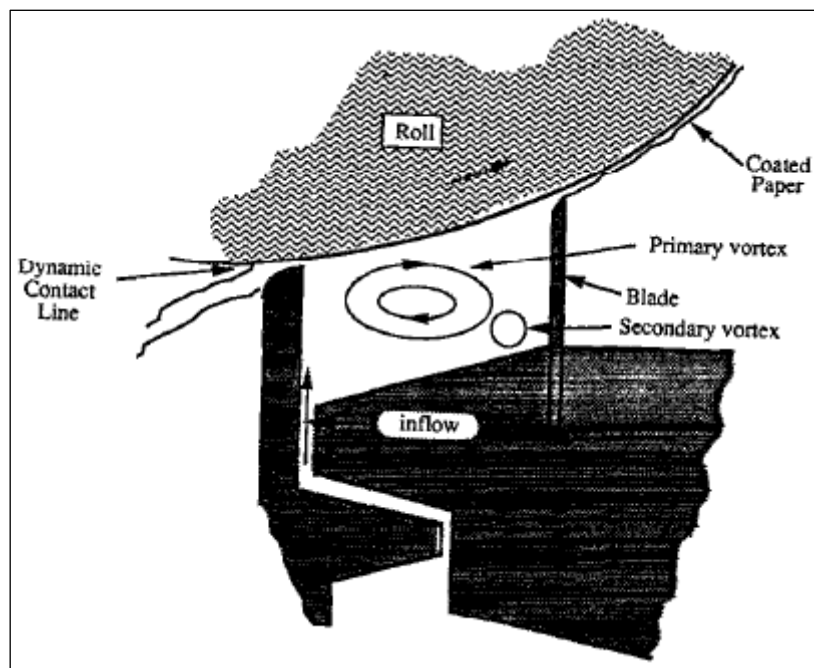


**Fig. 1:** Example of Driven Cavity Flow: Schematic of a Short-dwell Coater (from Aidun *et al.* [2])

Being a very simple problem, the stability of the flow can be easily studied for a confined geometry with closed streamlines [2]. This problem was first examined by Burggraf [4], who studied the flow inside a square cavity by solving the Navier-Stokes equations for a Reynolds number from 0 to 400 [2]. However, there are only a few literatures which showed appropriate benchmarking results.

This paper is concerned about the flow parameters and the flow field of an incompressible, viscous fluid. Since our main concern in the cavity flow is the secondary corner eddies and the primary vortices so the grids are taken as finer near the stationary walls of the cavity. The fluid is taken as air, so the properties like density and kinematic viscosity is kept constant. Since this study is made at different aspect ratio and Reynolds number, therefore the velocity of the top lid is calculated accordingly. The results are verified by that of a well-known benchmark Ghia *et al.* [5].

## LITERATURE REVIEW

Being a simple, yet very important problem in the field of fluid mechanics, lid driven cavity problem has been studied by researchers for over 50 years now. This is mainly because of the fact that many fluid mechanics phenomena

like streamline patterns, creeping motions, primary vortices, secondary corner vortices, instabilities and transition from laminar to turbulent within a simple geometry. This is clearly pointed out in the comprehensive review made by authors Shankar and Deshpande [6]. The review also brings out the advantage of the flow domain being unchanged when different Reynolds number is been studied.

As mentioned earlier, Burggraf [4] was the first to perform both analytical (based on a linearized model) and numerical study on the structure of flow in re-circulating eddies for two cases of simplified geometry. The effect of Reynolds number ( $Re \leq 400$ ) on the structure of the flow was analysed.

The most notable study has been done by Ghia *et al.* [5] in 1982, where the vorticity-stream function approach was chosen to solve the Navier-Stokes equation for a two-dimensional incompressible flow in a square cavity. The cavity problem was used as the basis to check the efficacy of the coupled strongly implicit multigrid (CSI-MG) method for high Reynolds number fine-mesh cavity flow. They made the study for Reynolds number ranging from 100 to as high as 10000 and on uniform mesh sizes of  $129 \times 129$  for  $Re \leq 3200$  and  $257 \times 257$  for

$5000 \leq Re \leq 10,000$ . The results depict clearly the primary vortex, the secondary vortices in both the bottom corners and for  $Re \geq 3200$  also in the top left corners.

Directing the mesh size sensitivity in their study, Ghia *et al.* affirmed that the values of stream function and vorticity at the vorticity centre are observed to be considerably more responsive to the mesh size than the velocity profiles.

Another prominent research was made by Erturk *et al.* [7] in 2005. They solved the incompressible Navier-Stokes equations by the stream function-vorticity approach using a uniform grid size of  $601 \times 601$  for  $Re \leq 21,000$  with a maximum absolute residuals of the governing equations less than  $10^{-10}$ . In the same year a fourth-order compact formulation on the stream function-vorticity approach was done by Erturk *et al.* [8] to solve the incompressible Navier-Stokes equations and provide them with fourth-order spatial accuracy. In 2007, Erturk *et al.* [9] performed the study on triangular cavities for various corner angles. There also has been some promising work on rectangular cavities. Since in many industrial applications, we come across cavities of various depths rather than square cavities, some researchers have studied cavities with various aspect ratios. Lin *et al.* [10] in 2010 used the multi relaxation time (MRT) Lattice Boltzmann equation (LBE) was at different Reynolds numbers (100–7500) and cavity aspect ratios (1–4). Their results clearly showed the merger of the bottom corner vortices into a primary vortex and the re-emergence of the corner vortices as the Reynolds number increases. These phenomenon were found to be more visible as the aspect ratio is increased; i.e. for deep cavities.

Another research performed by Pandit, 2007 [11], where a new method to solve two-dimensional Navier-Stokes equations for incompressible viscous flow inside irregular geometries beyond rectangular was proposed. The method is based on second order compact finite difference discretization of the fourth order stream function equation on computational plane. Kosinski *et al.* (2007)

[12] focused their study on the flow of incompressible fluid and solid particles inside a driven cavity. They have related the concept to applications like in pneumatic transport of dusts. The analysis is made by considering the solid particles as points moving in the computational domain due to fluid motion, thereby using the Eulerian-Lagrangian (E-L) approach to model the particle phase.

In 2006, Patil *et al.* [13] also used Lattice Boltzmann simulation to analyse the flow inside rectangular cavities for different Reynolds numbers. They computed the value of critical aspect ratio for Reynolds number 50, which was found in close agreement with the value predicted by numerical [14] result for the limits of creeping-flow and experiment by [15].

Thus we see that a lot of research has been done in this topic. Some of the most promising results are given by Ghia *et al.* [5], Erturk *et al.* [7] etc. for Reynolds number as high as 21000. These results are widely used as benchmark by many authors. Methods like stream function-vorticity, primitive variable approach, Lattice Boltzmann approach, etc. are mostly used. The coupled strongly implicit multigrid (CSI-MG) method used by Ghia *et al.* [5] is found to be one of the most prominent methods. There are by far more numerical results as compared to experimental results.

## MATHEMATICAL MODELLING

In order to numerically analyse this problem, we have used the commercially available CFD software ANSYS FLUENT (Academic Version 18.1).

### Problem Statement

The flow is assumed to be steady and two-dimensional. The fluid in the driven cavity is taken as air and so the density ( $\rho = 1 \frac{kg}{m^3}$ ) and the dynamic viscosity ( $\mu = 0.00002 \frac{kg}{s.m}$ ) are constant throughout the analysis. Figure 3.1 shows the schematic of the rectangular cavity. The cavity height and width is denoted as  $H$  and  $L$ , respectively and the aspect ratio ( $K$ ) is defined as  $K = \frac{L}{H}$ . Reynolds number is defined by  $Re = \frac{U_{lid} L}{\nu}$ ; where  $U_{lid}$  = velocity of the

moving lid,  $\nu$  = kinematic viscosity of the fluid and  $l$  = characteristic length of the cavity.

**Boundary and Initial Condition**

In this study, we have examined the cavity system with the following boundary and initial conditions (as shown in Figure 2):

- i) The top wall or lid of the cavity is moving with a uniform velocity ( $u=U_{lid}$ ,  $v=0$ ), which varies for different Reynolds number ( $Re = \frac{\rho U_{lid} L}{\mu}$ )
- ii) The left, right and bottom walls are considered to be stationary, which follows the state of no-slip boundary condition ( $u=0$ ,  $v=0$ ).

**Governing Equations**

In the present study, the cavity problem is governed by the Navier-Stokes equations and the continuity equation. The general form of equation for conservation of mass or the continuity equation can be written as follows:

$$\frac{\partial u}{\partial x} + \frac{\partial v}{\partial y} = 0 \tag{1}$$

Now, the conservation of momentum equation or the Navier-Stokes equation for two-dimensional incompressible flow can be written as follows:

**X-momentum Equation**

$$\rho \left[ u \frac{\partial u}{\partial x} + v \frac{\partial u}{\partial y} \right] = - \frac{\partial p}{\partial x} + \mu \left( \frac{\partial^2 u}{\partial x^2} + \frac{\partial^2 u}{\partial y^2} \right) \tag{2}$$

**Y-momentum Equation**

$$\rho \left[ u \frac{\partial v}{\partial x} + v \frac{\partial v}{\partial y} \right] = - \frac{\partial p}{\partial y} + \mu \left( \frac{\partial^2 v}{\partial x^2} + \frac{\partial^2 v}{\partial y^2} \right) \tag{3}$$

**Nomenclature:**

- $u$  = x-direction velocity
- $v$  = y-direction velocity
- $\mu$  = dynamic viscosity
- $Re$  = Reynolds number
- $\rho$  = density
- $p$  = pressure
- $V$  = velocity vector
- $K$  = aspect ratio
- $U_{lid}$  = velocity of the lid

**NUMERICAL METHOD**

In an effort to discretize the governing equations, a pressure-based approach in the ANSYS FLUENT software is used, where the pressure field is obtained by solving a pressure correction equation. This equation is formulated by manipulating continuity and momentum equations. This CFD software solves the governing integral equations for the conservation of mass and momentum [16]. For the linearization of the discretized equations and their solution, we have used the SIMPLE algorithm. SIMPLE is acronym for Semi-Implicit Method for Pressure Linked Equations [17]. This scheme is best used for steady state solution of laminar flow fields [18]. The flow chart of the SIMPLE algorithm [17] is shown in Figure 3.

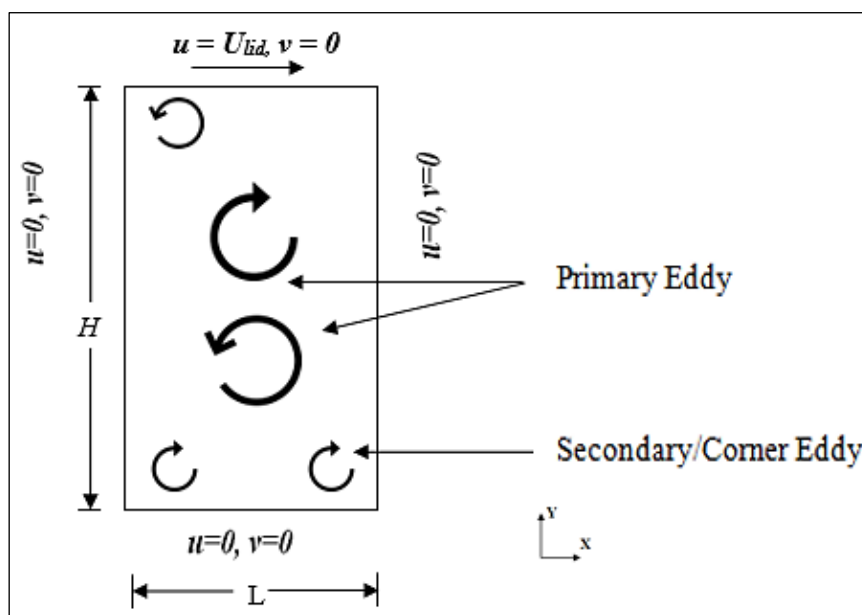


Fig. 2: Schematic of the Flow inside the Rectangular Cavity and the Boundary Conditions.

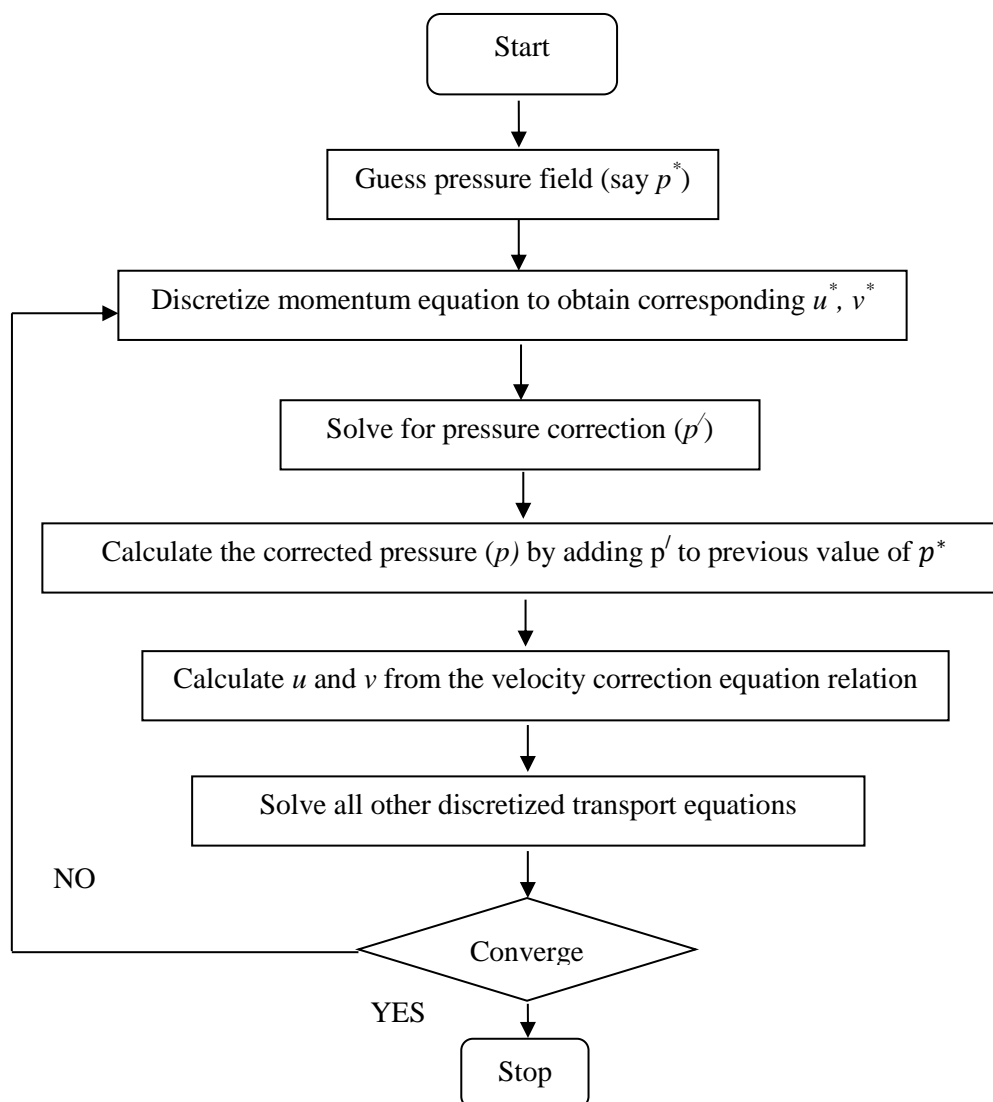


Fig. 3: Flowchart of SIMPLE Algorithm.

The iteration is manipulated to conclude when the scaled residual goes below or equal to  $10^{-8}$ . The results are found to have good agreement with those of Patil *et al.* [13], Pandit [11], Lin *et al.* [10] and Ghia *et al.* [5].

## RESULTS AND DISCUSSIONS

The method that is used for this study proves to be a viable alternative to investigate the flow inside a rectangular cavity. This is represented by the validation of the present results with the well-known benchmark by Ghia *et al.* [5]. Here we have compared the  $u$  and  $v$  velocity profiles at horizontal and vertical lines passing through the geometrical centre of the cavity. The comparison of results for Reynolds number 100, 1000 and 5000 at  $K=1$  are shown in Figure 4. The present results are found to have good agreement with the

reference. To compare the results we have used non-dimensional parameters which are as follows:

$$U = u/U_{lid}, V = v/U_{lid}, X = x/L, Y = y/L \quad (4)$$

Ghia *et al.* [5] mention the significance of these graphs. They pointed out the thinning of wall boundary layers with the increase in Reynolds number from these graphs. If we direct our attention towards the  $U$  versus  $Y$  profile (Figure 5), we can see that, the  $U$ -velocity for Reynolds number 5000 reaches a local maximum value at lower value of  $Y$  ( $Y \sim 0.075$ ) than that of Reynolds number 1000 ( $Y \sim 0.175$ ) and 100 ( $Y \sim 0.45$ ). They also indicated that the rate of thinning is very slow for  $Re \geq 5000$ . At  $K=1$ , Cartesian grid sizes are taken similar to that of Ghia *et al.* [5]. However, a grid independency test is done for

Reynolds number 1000 at  $K=1$ . We have compared the predicted values of  $U$  and  $V$  velocities at the mid-planes of the cavity for five different grid sizes i.e.  $65 \times 65$ ,  $129 \times 129$ ,  $257 \times 257$ ,  $514 \times 514$ ,  $710 \times 710$ , which are shown in Figure 6. It is found that mesh size of  $129 \times 129$  will give acceptable results, which is also seen from the results of the present study.

Also the streamline distribution of the flow inside the cavity ( $K=1$ ) is shown in Figure 7 for different Reynolds number. Lin *et al.* [10] pointed out the flow is found to be steady even at high Reynolds number 7500. The streamline patterns are found to be in close agreement

with that of Ghia *et al* [5]. As indicated by [5], [11], [10] and every author in this field, we can point out that the corner eddies increases in size as the Reynolds number increases. For low and moderate Reynolds numbers (e.g. 100, 400, and 1000), we can find only two secondary vortices in the corner of the cavity, but from  $Re=3200$  we can find a vortex in the top left corner of the cavity. Moreover, this vortex increases in size as the Reynolds number increases from 3200 (Figure 5 (e) and Figure 5 (f)). It is also observed that the vortices (both primary and secondary) change its position with the increase in Reynolds number.

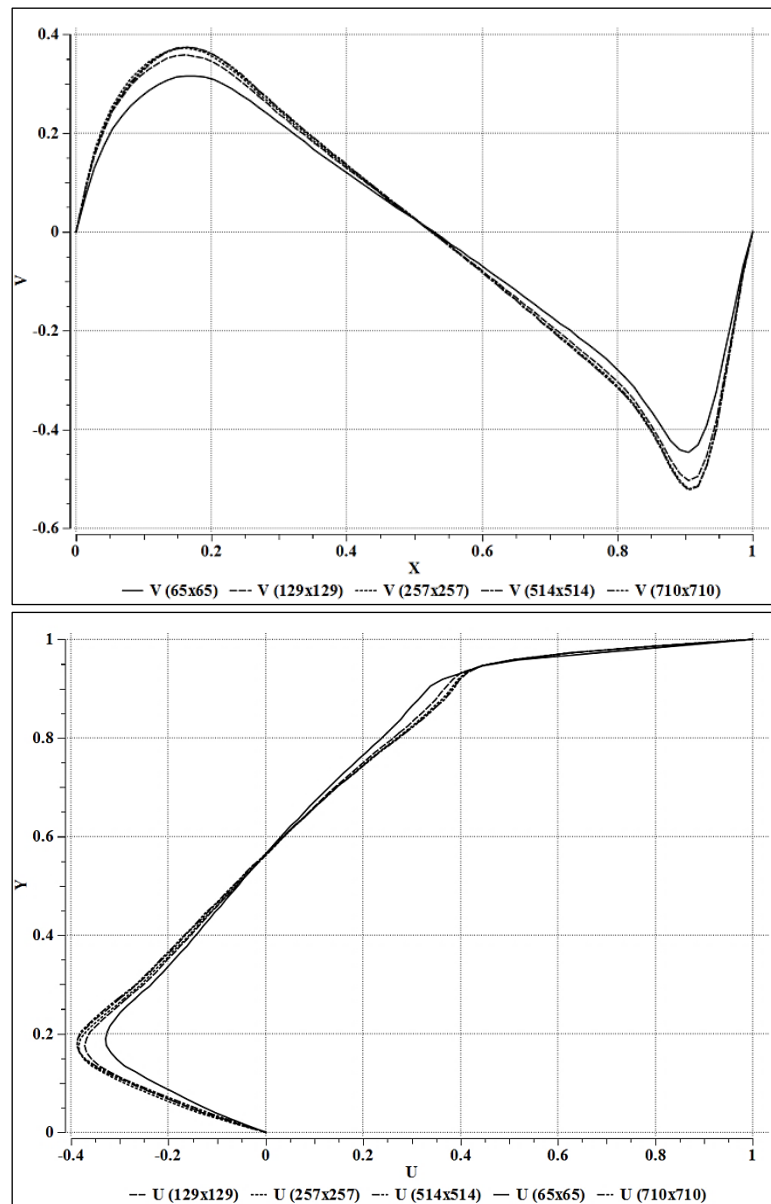


**Fig. 4:** Comparison of  $U$  and  $V$  Velocities at the Mid-Plane for Different Mesh Sizes for  $Re= 1000$ ,  $K= 1$ .

**Table 1:** Comparisons of Location of the Primary and Corner Vortices for different Reynolds Number with [5], [11] and [10] at  $K=1$ .

Reynolds Number	Primary Vortex		Left Corner Vortex		Right Corner Vortex	
	X	Y	X	Y	X	Y
<b>100</b>						
[5]	0.6172	0.7344	0.0313	0.0391	0.9453	0.0625
[11]	0.6184	0.7273	0.0316	0.0439	0.9425	0.0575
[10]	0.6140	0.7323	0.0346	0.0342	0.9448	0.0591
Present (129x129)	0.6160	0.7371	0.0338	0.0346	0.9436	0.0624
<b>400</b>						
[5]	0.5547	0.6055	0.0508	0.0469	0.8906	0.1205
[11]	0.5532	0.6055	0.0528	0.0439	0.8908	0.1384
[10]	0.5543	0.6024	0.0510	0.0468	0.8875	0.1206
Present (129x129)	0.5554	0.6060	0.0506	0.0467	0.8852	0.1212
<b>1000</b>						
[5]	0.5313	0.5625	0.0854	0.0781	0.8594	0.1094
[11]	0.5266	0.5532	0.0840	0.0840	0.8577	0.1092
[10]	0.5309	0.5645	0.0833	0.0776	0.8652	0.1117
Present (129x129)	0.5324	0.5656	0.0825	0.0766	0.8657	0.1124
<b>3200</b>						
[5]	0.5165	0.5469	0.0859	0.1094	0.8125	0.0859
[11]	--	--	--	--	--	--
[10]	0.5178	0.5396	0.0812	0.1195	0.8248	0.0843
Present (257x257)	0.5186	0.5392	0.0813	0.1191	0.8247	0.0843
<b>5000</b>						
[5]	0.5117	0.5352	0.0703	0.1367	0.8086	0.0742
[11]	--	--	--	--	--	--
[10]	0.5151	0.5349	0.0732	0.1365	0.8050	0.0730
Present (257x257)	0.5157	0.5346	0.0738	0.1354	0.8062	0.0732
<b>7500</b>						
[5]	0.5117	0.5322	0.0645	0.1504	0.7813	0.0625
[11]	--	--	--	--	--	--
[10]	0.5129	0.5317	0.0648	0.1519	0.7910	0.0655
Present (257x257)	0.5139	0.5318	0.0657	0.1510	0.7936	0.0664

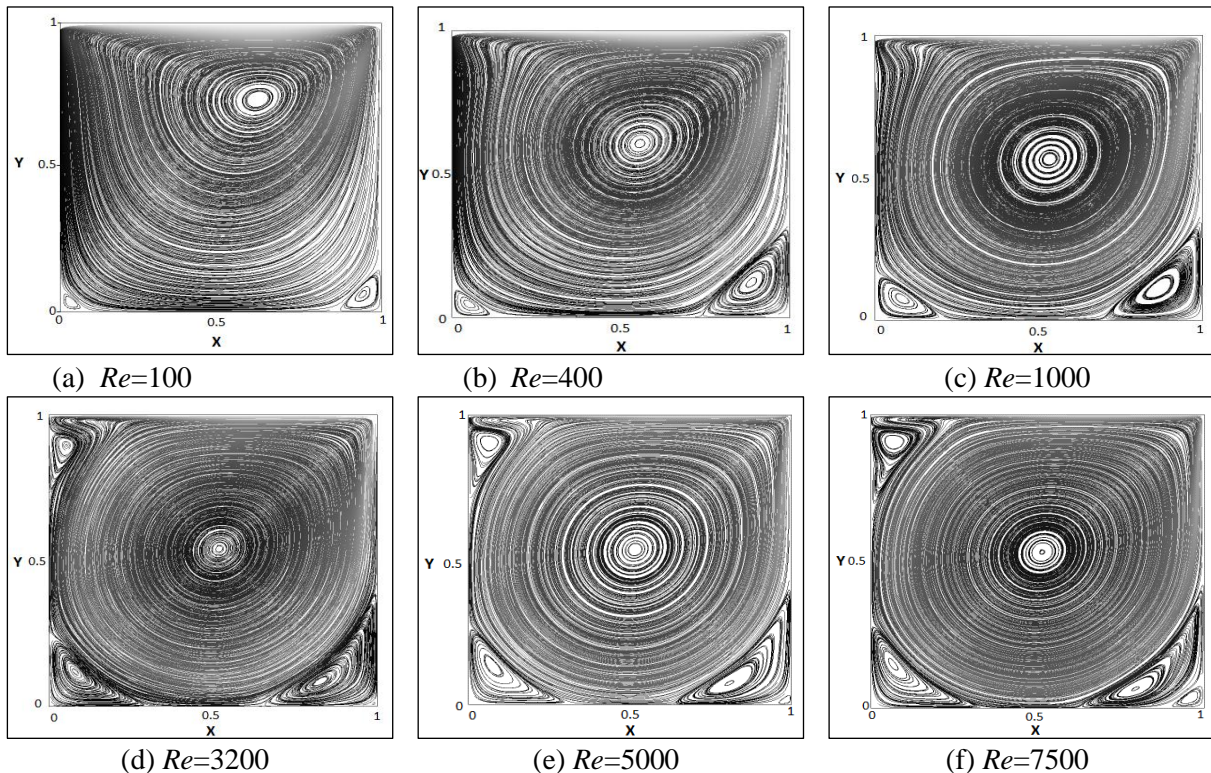


**Fig. 5:** Streamline Distribution Inside the Cavity of aspect Ratio  $K=1$  for Various Reynolds Number.

As seen in Figure 5 (a), the primary vortex is located in the upper right part of the cavity, and as the Reynolds number increases its position falls towards the geometrical centre of the cavity. From  $Re = 3200$ , the position is found to be almost constant for higher Reynolds number. The confidence towards this result is further strengthened by the positions of the vortices shown in Table 1. We can see that from  $Re = 3200$  the vertical and horizontal positions of the primary vortex from the end walls remain almost constant; changes being less than 1%.

Also regarding the secondary vortices, the right corner vortex tend to rise towards the left wall from  $Re=3200$  and the right corner vortex tend to fall towards left of the bottom wall. The above understanding can further be enlarged from the locations of the vortices provided in Table 1. Now we will present the study of cavity for aspect ratio  $K=1.5$ . We have simulated the results for  $Re = 100, 400, 1000, 3200,$  and  $5000$  using grid size of  $129 \times 193$  for  $Re= 100$  and  $400$ , and  $256 \times 384$  for  $Re= 1000, 3200$  and  $5000$ . The grid sizes are taken corresponding to the aspect ratio.

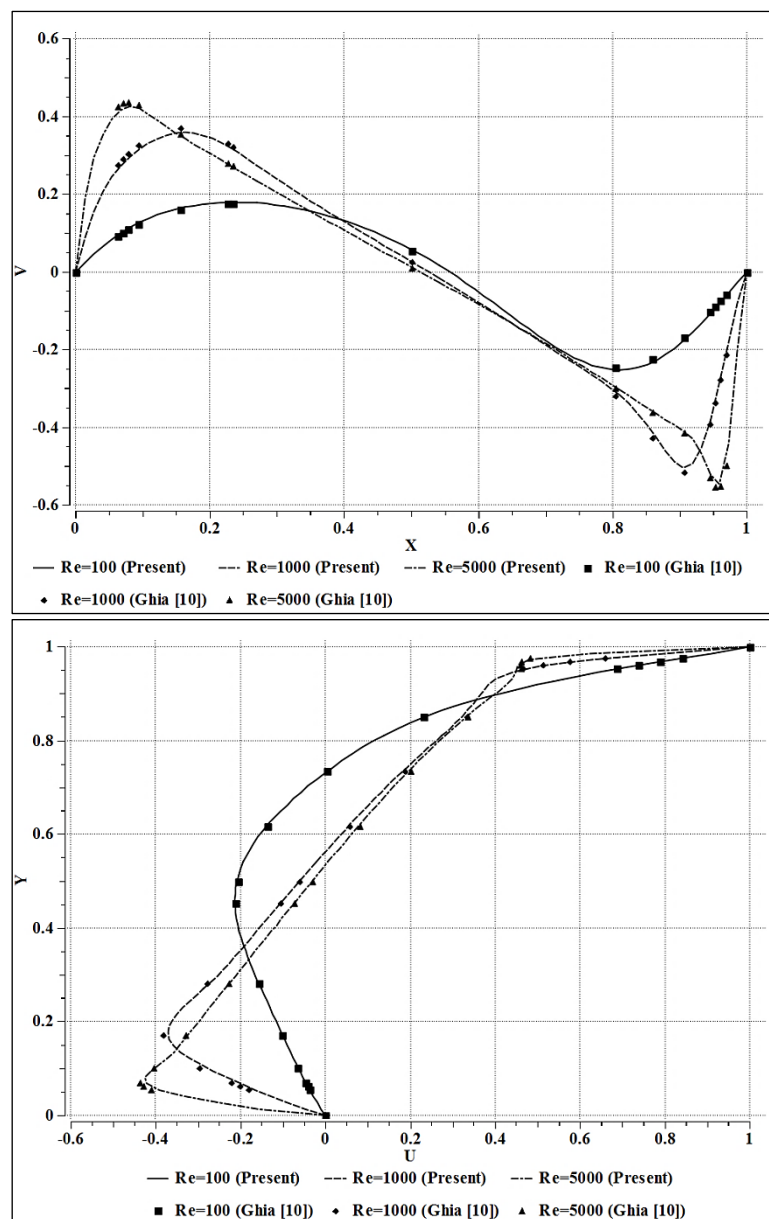


**Fig. 6:** Validation of  $U$  and  $V$  Velocities along the Vertical and Horizontal Line Passing through the Geometrical Centre of the Cavity, Respectively ( $K=1$ ).

Figure 7 shows the streamline distribution for different Reynolds number ( $K=1.5$ ). The results are seen to have good agreement with that of [13], [11] and [10]. As observed in [4], here too the steady state size of the corner vortices is found to increase as the aspect ratio is increased from  $K=1$  to  $K=1.5$  for  $Re=100$  (compare Figure 6(a) and 7(a)). Shankar and Deshpande [6] pointed out that, we can anticipate a sequence of counter-rotating eddies for a deep cavity and an infinite number of them in an infinite deep cavity. This is evident from the streamline pattern of  $K=1.5$  (Figure 8) which shows the formation of the second primary vortex as the Reynolds number is increased from 100 to 400, whereas

for the cavity of  $K=1$  (Figure 5) we could observe only one primary vortex.

The second primary vortex (for  $K=1.5$ ) is formed from the coalescence of the bottom corner vortices. If we bring our attention to Figure 7 (a), we can see that the corner vortices have grown large enough to merge into one counter-rotating primary vortex. Patil *et al.* [13] pointed out that the merging process is initiated by the formation of a stagnation point. Further increase in Reynolds number will initiate the formation of corner vortices as seen in Figure 7 (d) and (e). The coalescence of the corner vortices can also be seen when the aspect ratio is changed for a particular Reynolds number.

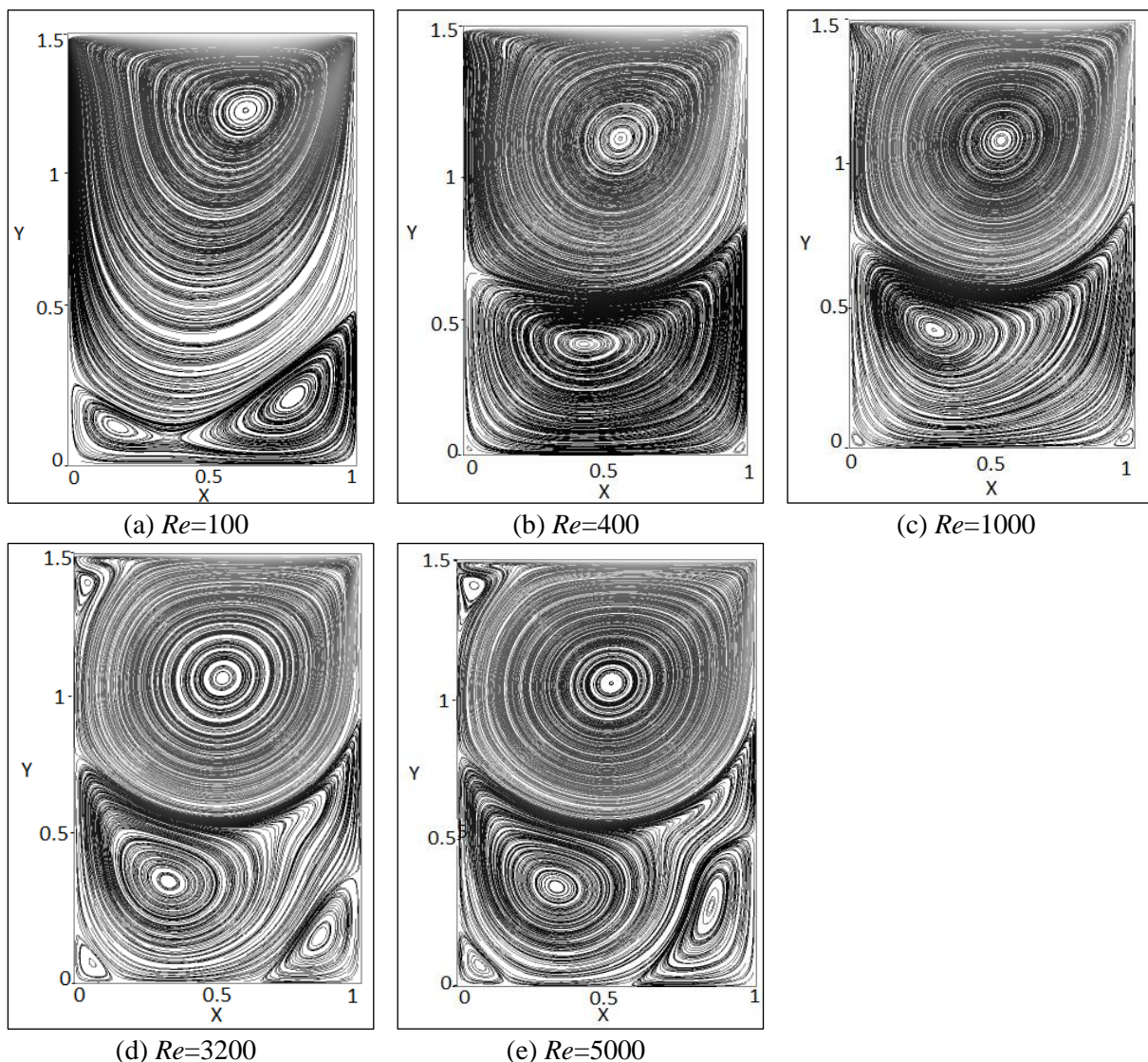


**Fig. 7:** Streamline Distribution Inside the Cavity of aspect Ratio  $K=1.5$  for Various Reynolds Number.

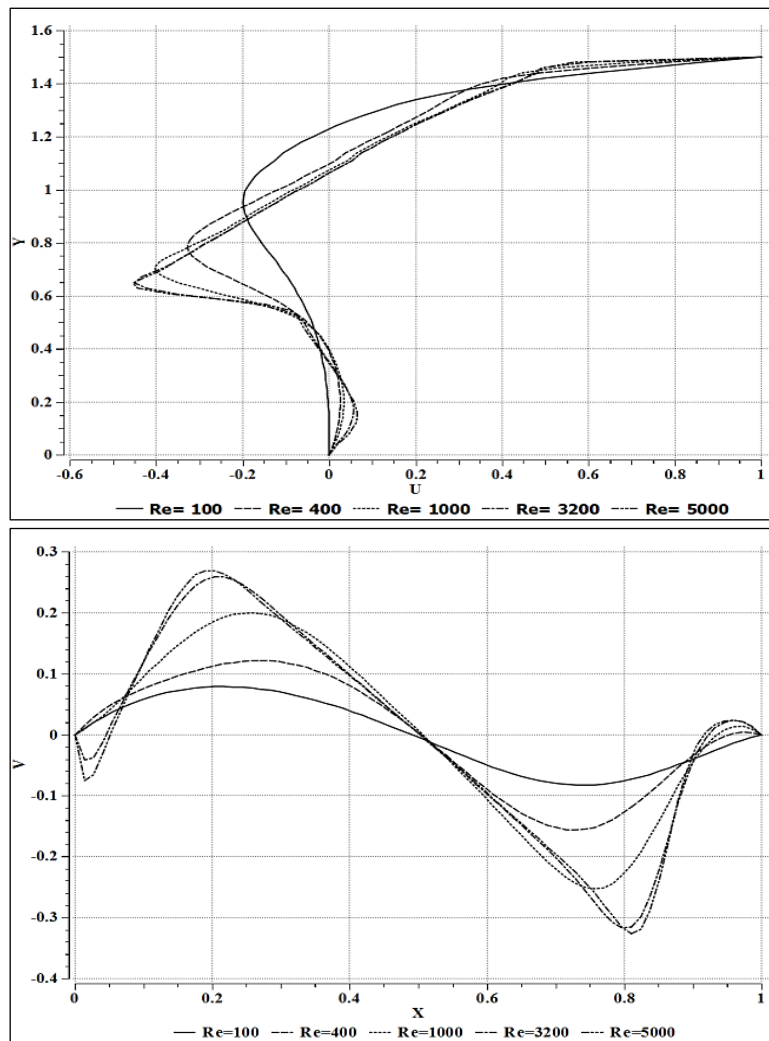


Fig. 8: Predicted U and V Velocities along the Vertical and Horizontal Line Passing through the Geometrical Centre of the Cavity, Respectively ( $K=1.5$ ).

Table 2: Comparisons of Location of the Primary and Corner Vortices for Different Reynolds Number with [13], [11] and [10] at  $K=1.5$ .

Reynolds Number	1 <sup>st</sup> Primary Vortex		2 <sup>nd</sup> Primary Vortex	
	X	Y	X	Y
<b>400</b>				
[13]	0.5625	1.1172	0.4453	0.3906
[11]	0.5399	1.1241	0.4205	0.3950
[10]	0.5522	1.1030	0.4259	0.3825
Present(129x193)	0.5542	1.1083	0.4260	0.3877
<b>1000</b>				
[13]	0.5352	1.0820	0.3007	0.4179
[11]	0.5399	1.0851	0.3439	0.3950
[10]	0.5293	1.0783	0.2960	0.4135
Present(256x384)	0.5301	1.0795	0.2966	0.4136
<b>3200</b>				
[13]	0.5195	1.0703	0.3320	0.3632
[11]	--	--	--	--
[10]	0.5175	1.0668	0.3293	0.3560
Present(256x384)	0.5185	1.0676	0.3296	0.3558
<b>5000</b>				
[13]	--	--	--	--
[11]	--	--	--	--
[10]	0.5151	1.0658	0.3322	0.3504
Present(480x720)	0.5163	1.0671	0.3330	0.3514

This gives rise to the concept of critical aspect ratio, which will be discussed latter in this section. From  $Re=3200$ , a vortex is formed in the top left corner of the cavity. The predicted velocities along the horizontal and vertical centrelines of the cavity are shown in Figure 8. Unlike the behaviour of the primary vortex in a square cavity to reach the geometry centre (Ghia *et al.* [5]), in case of deep cavities, the primary eddy does not fall towards the geometrical centre of the cavity. This is due to the formation of a secondary primary vortex which is evident for high Reynolds number, as explained by Patil *et al.* [13]. The location of the primary eddies for different Reynolds

number (as depicted in Table 2) also indicates the above behaviour.

We now extended our study to aspect ratio  $K=4$ . Here the most remarkable behaviour that can be seen is the coalescence of the two secondary eddies at the bottom as the Reynolds number is increased from 400 to 1000. This leads to the formation of the fourth primary eddy near the mid-plane of the cavity ( $X \sim 0.44$ ). Figure 9 shows the streamline distribution of the flow inside the cavity of  $K=4$  for different Reynolds number. The results are found to have good agreement with that of Lin *et al.* [10].

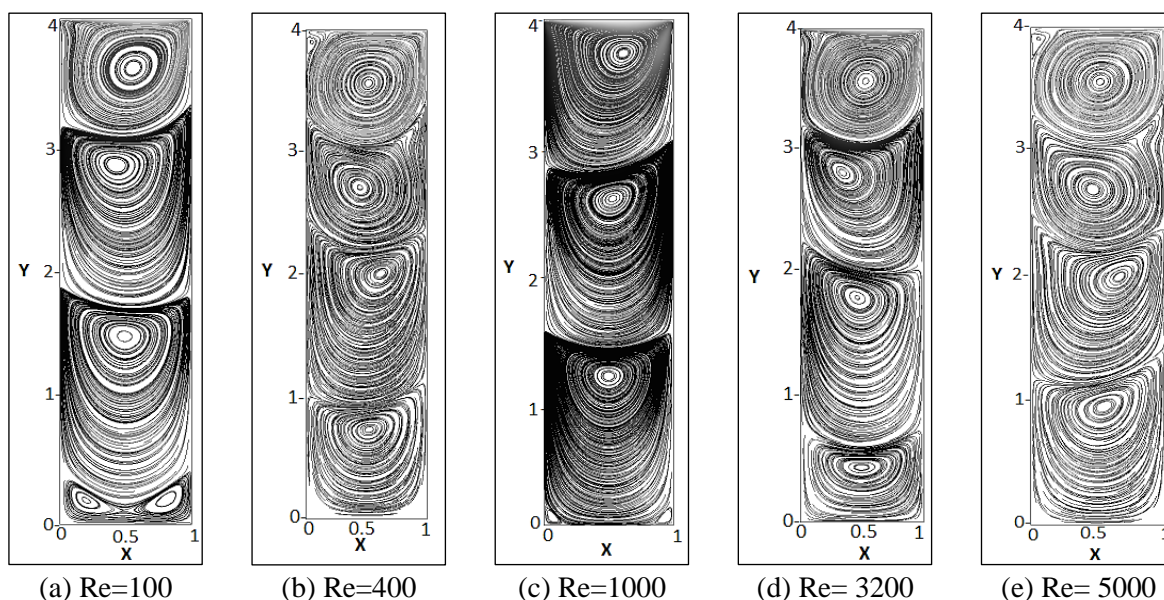
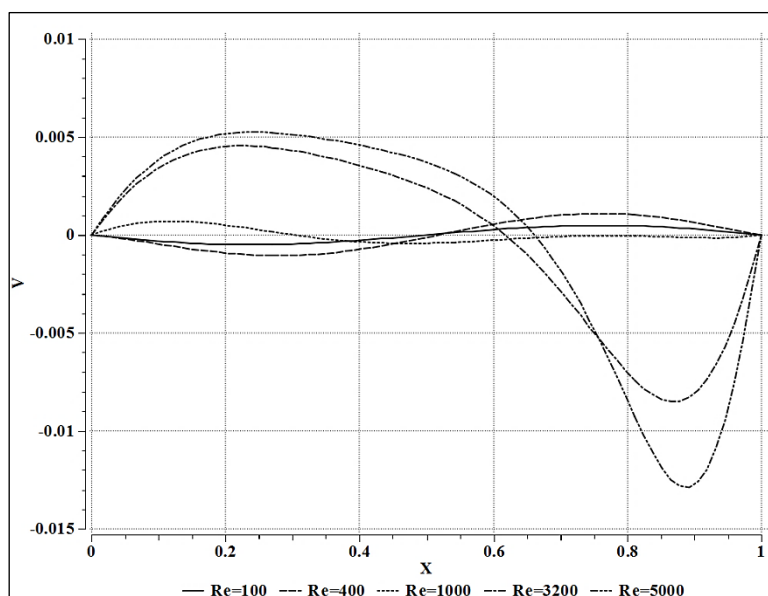


Fig. 9: Streamline Distribution Inside the Cavity of Aspect Ratio  $K=4$  for Various Reynolds Number.



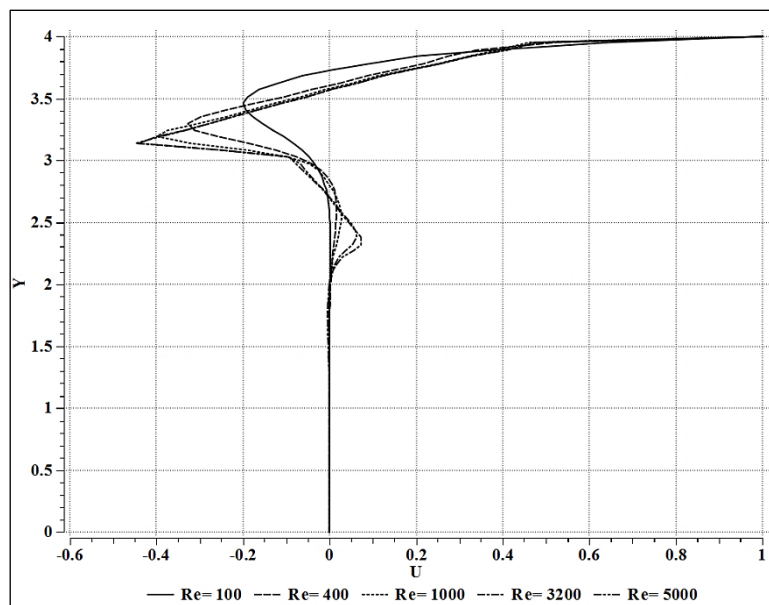


Fig. 10: Predicted *U* and *V* Velocities along the Vertical and Horizontal Line Passing through the Geometrical Centre of the Cavity, Respectively ( $K=4$ ).

Table 3: Comparisons of Location of the Primary and Corner Vortices for Different Reynolds Number with [13], [11] and [10] at  $K=1.5$ .

Reynolds Number	1 <sup>st</sup> Primary Vortex		2 <sup>nd</sup> Primary Vortex		3 <sup>rd</sup> Primary Vortex		4 <sup>th</sup> Primary Vortex	
	X	Y	X	Y	X	Y	X	Y
<b>400</b>								
[13]	0.5625	3.6172	0.4375	2.8515	0.5000	1.5000	--	--
[11]	0.5399	3.6029	0.4205	2.8750	0.5000	1.5266	0.5500	0.3300
[10]	0.5528	3.6039	0.4250	2.8378	0.4911	1.4875	--	--
Present (129x516)	0.5535	3.6088	0.4248	2.8460	0.4907	1.4879	--	--
<b>1000</b>								
[13]	0.5352	3.5820	0.3437	2.8515	0.4179	1.7734	--	--
[11]	0.5399	3.5834	0.3439	2.8750	0.4601	1.8801	0.5500	0.6667
[10]	0.5298	3.5778	0.3431	2.8356	0.4635	1.8167	0.5004	0.4385
Present (256x1024)	0.5300	3.5789	0.3452	2.8342	0.4632	1.8214	0.4982	0.4436
<b>3200</b>								
[13]	0.5195	3.5703	0.4453	2.7226	0.5937	1.9961	--	--
[11]	--	--	--	--	--	--	--	--
[10]	0.5172	3.5648	0.4465	2.7132	0.6215	2.009	0.5176	0.7247
Present (256x1024)	0.5174	3.5650	0.4473	2.7113	0.6172	2.007	0.5199	0.7278
<b>5000</b>								
[13]	--	--	--	--	--	--	--	--
[11]	--	--	--	--	--	--	--	--
[10]	0.5146	3.5650	0.4612	2.6996	0.6547	1.990	0.5750	0.9628
Present (256x1024)	0.5150	3.5660	0.4612	2.6991	0.6619	1.995	0.5761	0.9529

Also from the Figure 9, it evident the position of the first (top most) primary eddy eventually reach the mid-plane of the cavity ( $X \sim 0.51$ ). Table 3 show the location of all the four primaries eddies in the cavity and it is also compared with the results found by [13, 11, 10]. The predicted results from our study are found to have good agreement with them. Figure 10 shows the velocity profile graph in the mid-plane of the cavity of aspect ratio  $K=4$ .

Finally, discussed about the concept of critical aspect ratio ( $K_{cr}$ ) and predict the value of the same for various Reynolds number. Critical aspect ratio is defined as the value of aspect ratio when two secondary corner vortices coalesce together to form a new primary vortex [13]. Patil *et al.* [13] have reported the critical aspect ratio for  $Re=50$  to be  $1.64 \leq K_{cr} \leq 1.7$ . These result agree well with that of Shankar [14] who proposed a value of  $K_{cr}=1.8$  for the evolution of a second primary

eddy from the coalescence of two “Moffatt eddies”. We have also matched the same in our study (Figure 9). The streamline patterns for the same aspect ratio values are shown here and it is found to be in close agreement with the results of [13]. Since, the software and the method used prove to capture well the value of aspect ratio, so we have extended our study for two different Reynolds number. Patil *et al.* [13] anticipated that the value of  $K_{cr}$  will be lesser for higher Reynolds number. This has been clearly shown in the present simulations. Figure 10 and 11 shows the

results for critical aspect ratio for Reynolds number 100 and 400 respectively. These figures shows a series of streamline patterns which portray the change of the flow structure from the enlargement of the two secondary corner vortices (Figure 11 (a-c), 12 (a-c)) to the merging of one large primary vortex.

The critical aspect ratios for Reynolds number 100 and 400 are predicted to be  $K_{cr} \sim 1.54$  and 1.23 respectively. For Reynolds number of 400, the after-picture of Figure 12(d) can be observed in the Figure 12 (b) respectively.

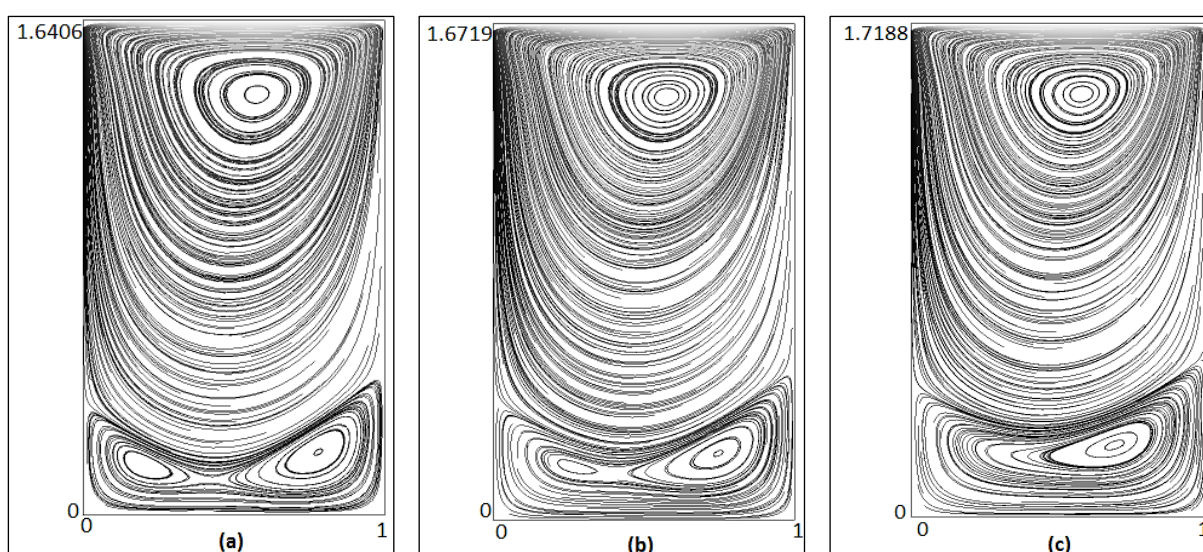


**Fig. 10:** Validation of Streamline Pattern for aspect Ratios  $K = 1.6406, 1.6719$  and  $1.7188$  for  $Re = 50$  with Patil *et al.* [13], Showing the Coalescence of the Two Secondary Vortices at Critical aspect Ratio ( $1.64 \leq K_{cr} \leq 1.7$ ).

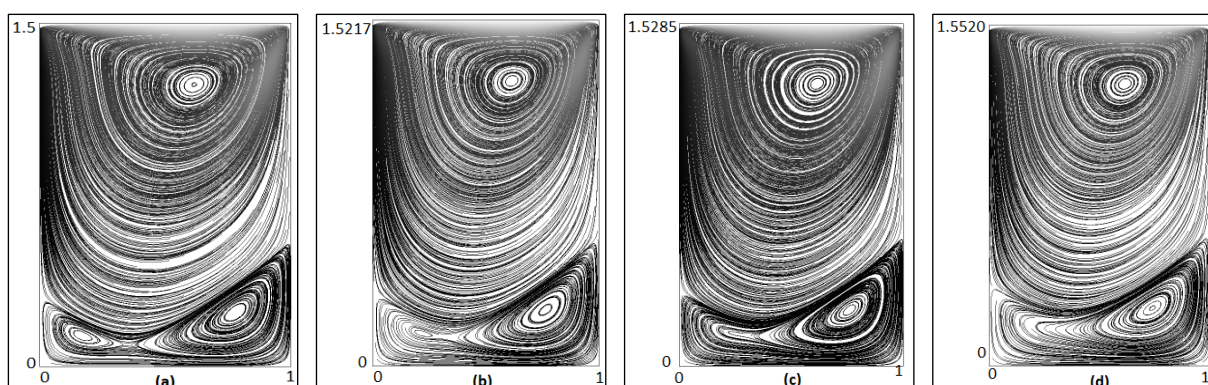


**Fig. 11:** Streamline Pattern for aspect Ratios  $K = 1.5, 1.5217, 1.5285$  and  $1.5520$  for  $Re = 100$ , Showing the Coalescence of the Two Secondary Vortices at Critical aspect Ratio ( $1.5285 \leq K_{cr} \leq 1.5520$ ).

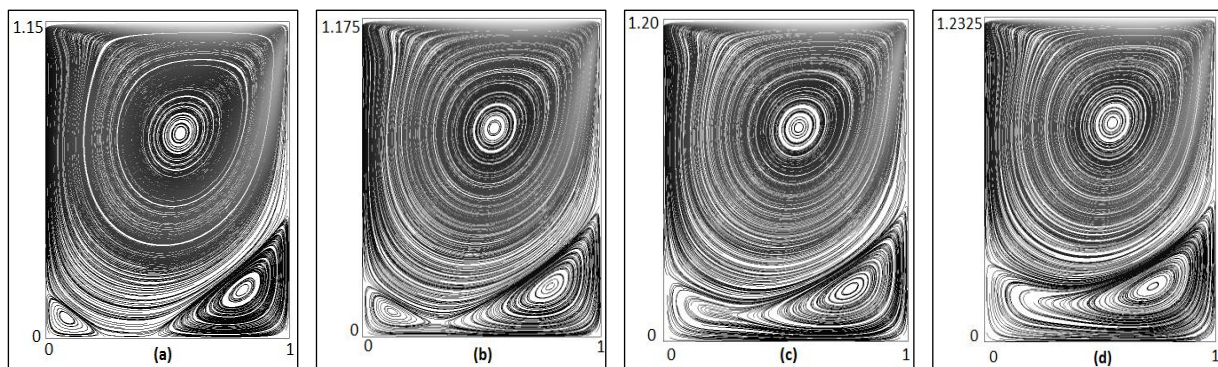


**Fig. 12:** Streamline Pattern for aspect Ratios  $K = 1.15, 1.175, 1.20$  and  $1.2325$  for  $Re = 400$ , Showing the Coalescence of the Two Secondary Vortices at Critical aspect Ratio ( $1.20 \leq K_{cr} \leq 1.2325$ ).

## CONCLUSION

In this study, we have investigated the flow inside different rectangular cavities for various Reynolds number. The numerical solution of 2D incompressible, steady Navier-Stokes equations are carried out in the CFD software ANSYS FLUENT (Academic Version 18.1) using the SIMPLE algorithm. The results are found to agree well with that of different prominent researchers. The formation and growth of secondary vortices are represented well by this analysis. The coalescence of bottom corner vortices to a new primary vortex with the increase in Reynolds number and also aspect ratio is successful. The software and the method used here proved to simulate well to match the results from other authors. Moreover, the structure of the topmost primary vortex is found to get less affected by Reynolds number for a particular aspect ratio. However, the location of the primary vortices are learnt to be affected, which can be realized from the detailed data mentioned in the three tables. Finally, a study has been made regarding the critical aspect ratio. The critical aspect ratio for Reynolds number of 100 and 400  $Re$ . This lid driven cavity problem has been studied for more than four decades and many important insights are given by many well-known authors. It is still believed to hold lots of details that is worth studying. This provides the motivation to increase the cognizance for both 2D and 3D flow.

## REFERENCES

- Zumbrunnen DA, Miles KC, Liu YH. Auto-processing of very fine scale composite materials by chaotic mixing of melts. *Composites Part A* 1995; 27A:37–47p.
- Aidun CK, Triantafillopoulos NG, Benson JD. Global stability of a lid-driven cavity with through flow: flow visualization studies. *Phys. Fluids A* 3:2081–91; 1991.
- Spasov Y, Herrero J, Grau FX, Giralt F. Linear stability analysis and numerical calculations of the lid-driven flow in a toroidally shaped cavity. *Physics of Fluids*. 2003; 15: 134p.
- Burggraf OR. Analytical and numerical studies of the structure of steady separated flows. *J Fluid Mech*. 1966; 24(1): 113p.
- Ghia U, Ghia KN, Shin CT. High-Re solutions for incompressible flow using Navier–Stokes equations and a multigrid method. *J Comput Phys*. 1982; 48: 387p.
- Shankar PN, Deshpande MD. Fluid mechanics in the driven cavity. *Ann Rev Fluid Mech*. 2000; 32: 93p.
- Erturk E, Gokcol C. Fourth-order compact formulation of Navier–Stokes equations and driven cavity flow at high Reynolds numbers. *Int. J. Numer. Meth. Fluids*. 2006; 50:421–436p.
- Erturk E, Corke TC., Gokcol C. Numerical Solutions of 2-D Steady Incompressible Driven Cavity Flow at High Reynolds Numbers. *Int. J. Numer. Meth. Fluids*. 2005 48: 747–774p.
- Erturk E, Gokcol C. Fine grid numerical solutions of triangular cavity flow. *Eur. Phys. J. Appl. Phys*. 2007; 38: 97–105p.
- L.-S. Lin, Y.-C. Chen, C.-A. Lin, Multi relaxation time lattice Boltzmann simulations of deep lid driven cavity flows at different aspect ratios. *Comput. Fluids*. 2011; 45: 233–240p.

11. Pandit SK. On the use of compact stream function-velocity formulation of steady Navier–Stokes equations on geometries beyond rectangular. *J Sci Comput.* 2008; 36: 219p.
12. Kosinski P., Kosinska A., Hoffmann A.C. Simulation of solid particles behaviour in a driven cavity flow. *Powder Technology.* 2009; 191: 327–339p.
13. Patil D, Lakshmisha K, Rogg B. Lattice Boltzmann simulation of lid-driven flow in deep cavities. *Comput Fluids.* 2006; 35: 11–16p.
14. Shankar PN. The eddy structure in Stokes flow in a cavity. *J. Fluid Mech.* 1993; 250:371–83p.
15. Hellou M, Coutanceau M. Cellular Stokes flow induced by rotation of a cylinder in a closed channel. *J. Fluid Mech.* 1992; 236:557–77p.
16. ANSYS® ANSYS Student Workbench, Release 18.1, Help System, Theory Guide, ANSYS, Inc.
17. Patankar SV. Numerical heat transfer and fluid flow. Hemisphere Publishing Corporation.
18. Barton I.E. Comparison of simple- and piso-type algorithms for transient flows. *International Journal for Numerical Methods in Fluids.* 1998; 26: 459–483p.

#### **Cite this Article**

Pantha Pradip Das, Kalyan Kumar Das. Numerical Investigation of Fluid Flow Inside A Rectangular Driven Cavity at Moderate Reynolds Numbers. *Journal of Aerospace Engineering & Technology.* 2017; 7(3): 46–60p.